

Astragaloside IV ameliorates diabetic nephropathy in *db/db* mice by inhibiting NLRP3 inflammasome-mediated inflammation

HUI FENG^{1,2}, XIAOYUN ZHU², YANG TANG³, SHOUQIANG FU³, BINGTAN KONG² and XIMING LIU²

¹School of Chinese Medicine, School of Integrated Chinese and Western Medicine, Nanjing University of Chinese Medicine, Nanjing, Jiangsu 210023; ²Department of Laboratory of Diabetes, Guang'anmen Hospital, China Academy of Chinese Medical Sciences, Beijing 100053; ³School of Chinese Medicine, Beijing University of Chinese Medicine, Beijing 100029, P.R. China

Received December 14, 2020; Accepted May 31, 2021

DOI: 10.3892/ijmm.2021.4996

Abstract. Diabetic nephropathy (DN) is a primary cause of end-stage renal disease. Despite the beneficial effects of astragaloside IV (AS)-IV on renal disease, the underlying mechanism of its protective effects against DN has not been fully determined. The aims of the present study were to assess the effects of AS-IV against DN in *db/db* mice and to explore the mechanism of AS-IV involving the NLR family pyrin domain containing 3 (NLRP3), caspase-1 and interleukin (IL)-1 β pathways. The 8-week-old *db/db* mice received 40 mg/kg AS-IV once a day for 12 weeks via intragastric administration. Cultured mouse podocytes were used to further confirm the underlying mechanism *in vitro*. AS-IV effectively reduced weight gain, hyperglycemia and the serum triacylglycerol concentration in *db/db* mice. AS-IV also reduced urinary albumin excretion, urinary albumin-to-creatinine ratio and creatinine clearance rate, as well as improved renal structural changes, accompanied by the upregulation of the podocyte markers podocin and synaptopodin. AS-IV significantly inhibited the expression levels of NLRP3, caspase-1 and IL-1 β in the renal cortex, and reduced the serum levels of tumor necrosis factor (TNF)- α and monocyte chemoattractant protein-1. In high glucose-induced podocytes, AS-IV significantly improved the expression levels of NLRP3, pro-caspase-1 and caspase-1, and inhibited the cell viability decrease in a dose-dependent manner, while NLRP3 overexpression eliminated the effect of AS-IV on podocyte injury and the inhibition of the NLRP3 and caspase-1 pathways. The data obtained from *in vivo* and *in vitro* experiments demonstrated that AS-IV ameliorated renal functions and

podocyte injury and delayed the development of DN in *db/db* mice via anti-NLRP3 inflammasome-mediated inflammation.

Introduction

Diabetic nephropathy (DN) is a characteristic microvascular complication of diabetes mellitus (DM). In total, ~30% of patients with type 1 DM and 40% of those with type 2 DM (T2DM) further develop DN (1). DN is the leading cause of end-stage renal disease and a major cause of mortality in patients with DM (2). Proteinuria is a typical clinical feature of DN that is associated with a substantial risk of progressive kidney damage (2). Podocytes, which are highly differentiated glomerular epithelial cells, are critical for maintaining glomerular filtration function. Podocyte injury is closely associated with glomerular sclerosis, increased proteinuria and loss of renal function, all of which are crucial to the progression of DN (3). Although various medications have been used to control blood glucose and blood pressure, reduce proteinuria and improve renal function, the increased urinary albumin excretion and decreased evaluation of glomerular filtration rate still increase the risk of DN (4). Thus, the underlying mechanisms of action and treatment strategies for DN need to be further investigated.

Multiple studies have confirmed that inflammation, induced by the NLR family pyrin domain containing 3 (NLRP3) inflammasome, is crucial in the improvement of DN (5,6). Inflammasomes are macromolecular complexes consisting of a sensor molecule, the adaptor apoptosis-associated speck-like protein containing a caspase recruitment domain (ASC) and the effector protease pro-caspase-1, which trigger central and rapid inflammatory responses to cytosolic insults (7). The NLRP3 inflammasome is currently the most characterized inflammasome. Activated NLRP3 can recruit ASC to promote the conversion of pro-caspase-1 to active caspase-1, which is crucial for the maturation of interleukin (IL)-1 β and IL-18 (8). The NLRP3 inflammasome activation primarily in renal resident cells including podocytes is crucial to the establishment of DN (6). Considerable NLRP3 inflammasome activation has been demonstrated in patients with T2DM, and its inhibition or NLRP3 deficiency can protect against podocyte injury and delay the progression of DN (9). IL-1 β is a pleiotropic

Correspondence to: Professor Ximing Liu, Department of Laboratory of Diabetes, Guang'anmen Hospital, China Academy of Chinese Medical Sciences, 5 Beixiange Road, Beijing 100053, P.R. China
E-mail: lxmhospital@126.com

Key words: diabetic nephropathy, astragaloside IV, proteinuria, podocyte, NLR family pyrin domain containing 3 inflammasome, inflammation

pro-inflammatory cytokine that can induce other inflammatory mediators, such as IL-6, tumor necrosis factor (TNF)- α and monocyte chemoattractant protein-1 (MCP-1), which are also closely associated with the progression of DN (10,11). Hence, targeting the NLRP3, caspase-1 and IL-1 β pathways could be an effective treatment strategy for the management of DN.

Astragaloside IV (AS-IV) is a key active component of *Astragalus membranaceus* (Fisch.) Bge, which is an herbaceous perennial widely used in Traditional Chinese medicine. AS-IV has been used to treat several complications related to diabetes, including DN, cardiovascular diseases and diabetic retinopathy (12,13). The protective effects of AS-IV have been linked to its diverse bioactive properties, including anti-inflammatory and antioxidant effects (14). A recent study has suggested that AS-IV can inhibit NLRP3 inflammasome activation, thus protecting against high glucose-induced endothelial cell injury (15). Thus, AS-IV ameliorates DN likely by inhibiting NLRP3 inflammasome-mediated inflammation.

The aim of the present study was to evaluate the protective effects of AS-IV on the progression of DN in *db/db* mice, a T2DM mouse model with similar kidney lesions to those observed in patients with DN (16), and analyze the expression levels of NLRP3, caspase-1 and IL-1 β *in vivo* and *in vitro* to determine whether AS-IV ameliorates DN by inhibiting NLRP3 inflammasome-mediated inflammation.

Materials and methods

Chemicals and reagents. AS-IV (high-performance liquid chromatography ≥ 98 0%; cat. no. 180408) was purchased from Chengdu King-tiger Pharm-chem. Tech. Co., Ltd. Benazepril (cat. no. X2689) was purchased from Novartis International AG. The mouse albumin ELISA kit (cat. no. CSB-E1387m) was purchased from Cusabio Technology LLC. The Coomassie Brilliant Blue kit was purchased from Nanjing Jiancheng Bioengineering Institute. The BCA protein assay kit (cat. no. P1511) was purchased from Applygen Technologies, Inc. The rabbit anti-NLRP3 (product code ab214185) antibody was purchased from Abcam, the caspase-1 (cat. no. 22915-1-AP) antibody from ProteinTech Group, Inc. and the anti-podocin antibody (cat. no. BS90960) from Bioworld Technology, Inc. β -Actin (product no. 4970) and anti-rabbit IgG HRP-linked antibodies (product no. 7074S) were purchased from Cell Signaling Technology, Inc. Mouse anti-synaptopodin (cat. no. sc-515842) was purchased from Santa Cruz Biotechnology, Inc. Fluorescent mounting medium with DAPI (cat. no. ZLI-9557), Alexa-488-labeled goat anti-rabbit antibody (cat. no. ZF-0511), and Alexa-594-labeled goat anti-mouse antibody (cat. no. ZF-0513) were purchased from ZSGB-BIO; OriGene Technologies. TRIzol[®] (cat. no. 15596-026) and RevertAid First Strand cDNA Synthesis kit (cat. no. K1622), and Alexa-488-labeled donkey anti-mouse antibody (cat. no. A32766) were purchased from Invitrogen; Thermo Fisher Scientific, Inc. Power SYBR[™] Green PCR Master mix (cat. no. A25742) was purchased from ABI, Inc.; Thermo Fisher Scientific, Inc. Super ECL detection reagent (cat. no. 36208ES60) was obtained from Yeasen Biotechnology (Shanghai) Co., Ltd. and recombinant murine γ -interferon (cat. no. 96-315-05) from PeproTech, Inc.

Animals and treatment. Male 6-week-old BKS-Leprem2Cd479/Nju (*db/db*; n=30; weight, 35-40 g) and C57BL/Ksj (wild-type, WT; n=10; weight, 18-20 g) mice were purchased from the Model Animal Research Center of Nanjing University [Nanjing, China; approval no. SCXK (SU) 2015-0001]. The animals were maintained at the Animal Center of Guang'anmen Hospital (living conditions, 24 \pm 2°C; 60-80% relative humidity; 12-h light/dark cycle). All mice were given free access to standard mice chow and drinking water. After 2 weeks of acclimatization, the *db/db* mice were randomly divided into three groups (n=10). Each group was then administered either vehicle (distilled water, 10 ml/kg), benazepril (10 mg/kg) or AS-IV (40 mg/kg) (17) once a day via gavage. A total of 10 WT mice were administered vehicle alone. The experiment lasted for 12 weeks.

During the experiment, body weight was measured once a week. Every three weeks, all mice were fasted for 6 h to assess fasting blood glucose (FBG). Next, 24-h urine samples were collected using individual metabolic cages on the last 3 experimental days. All mice were anesthetized with isoflurane inhalation and euthanized by exsanguination after 12 weeks of administration. Anesthesia was induced by inhalation of isoflurane overdose (4%) and maintained with isoflurane (2%) inhalation in an isoflurane vaporizer (18). Pinch reflex examination was monitored to ensure full anesthesia. Blood samples (1-2 ml) for serum assessment were collected by cardiac puncture after confirming anesthesia. Respiratory and cardiac arrest and the absence of reflexes were used to ensure death. The kidney was removed quickly after confirming death. The kidney index was determined as follows: Kidney/body weight (g/kg). The renal cortex was carefully separated. Renal cortex tissues (1 mm³) were fixed in 4% glutaraldehyde for 4 h at 4°C for transmission electron microscopy (TEM) assays. Some tissues were fixed in 4% paraformaldehyde for 24 h at 4°C for histological, immunohistochemical, and immunofluorometric assays. The other tissues were frozen in liquid nitrogen and stored at -80°C for further analyses. The procedures for animal experimentation were in accordance with the guidelines of the Guang'anmen Hospital, Chinese Academy of Traditional Chinese Medicine (approval no. IACUC-GAMH-2019-010), and adhered to the Guide for the Care and Use of Laboratory Animals published by the United States National Institutes of Health (NIH Publication no. 85-23, revised 1996).

Construction of lentiviral vector and lentivirus packaging. The lentiviral vector overexpressing the NLRP3 gene (NLRP3-ov) and its empty vector (control-ov) were constructed and provided by Shanghai Genechem, Inc. (cat. no. GXDL0222696). In brief, chemical synthesis was used to produce DNA full-length of NLRP3 transcript (NM_001359638.1) and further cloned it into pLV[Exp]-copGFP:T2A:Puro-CMV>Shuttle lentiviral empty vector with 5'-flank *NheI* and 3'-flank *NotI* single restriction endonuclease enzymes, and finally generated overexpressing plasmid pLV[Exp]-copGFP:T2A:Puro-CMV>mNlrp3[NM_001359638.1]/FLAG. All of the positive clones were confirmed by DNA sequencing. Additionally, 293T packaging cells (cat. no. CRL3216; ATCC) from liquid nitrogen were quickly thawed, seeded into a 10-cm diameter dish and passed two generations before transfection. At the transfection step, the NLRP3 plasmid was mixed with two

packaging plasmids psPAX2 (cat. no. 12260) and pMD2.G (cat. no. 12259; both from Addgene, Inc.) at a ratio of 4:3:3 (4 μ g:3 μ g:3 μ g), and co-transfected into 293T cells at 70% confluence using jetPRIME[®] transfection reagent (reference no. 114-75; Polyplus-transfection SA) according to the manufacturer's instructions. Each viral supernatant was harvested ~48 h later and centrifuged at 5,000 x g for 1.5 h at 4°C in a Beckman ultracentrifuge. The negative control lentivirus was prepared using the same method, respectively.

Cell culture and transfection. The conditional immortal mouse podocytes were kindly donated by Professor Weijing Liu from Dongzhimen Hospital, Beijing University of Chinese Medicine and were cultured as previously described (19). Briefly, after podocytes were cultured at 33°C in RPMI-1640 medium (Gibco; Thermo Fisher Scientific, Inc.) containing 100 U/ml recombinant murine γ -interferon, they were cultured in medium without recombinant murine γ -interferon to promote differentiation at 37°C for 7 days. The immunofluorescence of synaptopodin, a marker protein of process formation differentiation of podocytes, was used to authenticate the differentiation and maturation of podocytes. Next, podocytes were divided into five groups: The control (podocytes treated with 5.5 mM glucose), high glucose (HG, podocytes treated with 50 mM glucose), 10- μ M AS-IV, 20- μ M AS-IV and 40- μ M AS-IV groups. When podocytes reached 60% confluence, groups were incubated with HG for 24 h (20) except for the control group. Drug treatment groups were pre-treated with different doses of AS-IV (10, 20 and 40 μ M) at 37°C for 24 h prior to HG administration. Finally, podocytes in each group were collected for the following examination. Next, to determine the effect of AS-IV on NLRP3 in HG-induced podocyte injury, podocytes were infected with NLRP3-ov vector at a multiplicity of infection (MOI) of 20 using Lipofectamine[®] 3000 for 4 h. The medium was replaced with fresh culture medium after transfection, and podocytes were harvested for subsequent studies at 24 h after transfection. Subsequently, podocytes were treated with 50 μ M D-glucose for 24 h in the absence or presence of 40 μ M AS-IV. The control-ov vector was also used as aforementioned.

MTT assay. Podocytes were placed in a 96-well plate at a density of 1x10⁵ cells/well. Podocytes were treated with vehicle and indicated concentrations of AS-IV (10, 20 and 40 μ M) in medium at 37°C for 24 h. Following incubation, the cell cultures were mixed with MTT solution at 37°C for 4 h. Then MTT solution was removed and dimethyl sulfoxide was added to dissolve the formazan crystals and absorption was measured at 570 nm on a spectrophotometer (NanoDrop Technologies; Thermo Fisher Scientific, Inc.).

Biochemical characteristics in the urine and serum. The urinary albumin concentration was determined using the mouse albumin ELISA kit, according to the manufacturer's instructions. Urinary total protein was measured using Coomassie Brilliant Blue staining reagent. Serum total cholesterol (TC), triacylglycerol (TG), high-density lipoprotein cholesterol (HDL-C), low-density lipoprotein cholesterol (LDL-C), blood urea nitrogen (BUN) and

urinary creatinine levels were assessed using an automatic biochemical analyzer (cat. no. AU5821; Beckman Coulter, Inc.). Albumin-to-creatinine ratio (ACR) was used to evaluate urinary albumin excretion (21). Creatinine clearance rate (Ccr) was used to determine the glomerular filtration rate (17). Ccr (ml/min) was calculated as follows: (Urinary creatinine/serum creatinine) x 24-h urine volume (ml)/1,440.

Histological analysis. Paraffin-embedded tissues were sectioned into 4- μ m-thick slices and placed onto slides. The slides were stained with hematoxylin and eosin, periodic acid-Schiff and Masson's trichrome staining to evaluate glomerular alteration. Histological tissue damage to the kidney was observed using a Nikon ECLIPSE Ti-S inverted light microscope (Nikon Corporation). In each section, 10 renal glomerular areas were measured using ImageJ software (version 1.52; National Institutes of Health) to calculate the mean glomerular cross-sectional area. The glomerular volume was calculated using the Weibel-Gomez technique with the following formula: Glomerular volume=Area^{1.5} x 0.75+0.21 (22). The fibrotic area in the glomeruli was calculated using Masson's trichrome staining.

TEM. Renal cortex tissues were fixed with 4% glutaraldehyde solution for 1 h at 4°C followed by 1% osmic acid for 2 h at 4°C. The samples were then dehydrated in gradient acetone, embedded in an Epon/Araldite mixture for 2 h at 25°C, sectioned into 50-nm-thick slices and stained with uranyl acetate and lead citrate for 30 min at 25°C. A TEM (cat. no. H-7650; Olympus Corporation) was used to perform TEM analysis. The ultrastructural changes, including glomerular basement membrane (GBM) thickness and foot processes width, were determined as previously described (23).

Luminex assays. The serum levels of IL-1 β , IL-6, TNF- α and MCP-1 were detected using Mouse High Sensitivity T Cell Magnetic Bead Panel with a Luminex 200 system (Luminex Corporation) as previously described (24) and following the manufacturer's instructions.

Immunofluorometric analysis. Double immunofluorescence was performed to localize NLRP3 and caspase-1 within podocytes in the kidney tissues. Following xylene dewaxing and gradient ethanol hydration, 4- μ m paraffin sections were subjected to antigen repair by heat mediation using citrate buffer (pH 6.0) at 95°C for 20 min and permeabilized with 0.3% Triton X-100 in Tris-buffered saline at 25°C for 10 min. Following washing thrice with PBS (5 min per wash), the slides were blocked with 10% goat serum for 2 h at 25°C and incubated overnight at 4°C with either mouse anti-synaptopodin (1:50) and rabbit anti-NLRP3 (1:50) antibodies, or mouse anti-synaptopodin (1:50) and rabbit anti-caspase-1 (1:100) antibodies. In addition, the slides were incubated overnight at 4°C with rabbit anti-podocin antibody (1:200) alone to assess podocyte injury. Following washing thrice with TBS (5 min per wash), these slides were incubated with Alexa-488-labeled and (or) Alexa-594-labeled secondary antibodies (1:50) for 1 h at 25°C in a humidified chamber. *In vitro*, podocytes were cultured on glass slides in a 12-well plate for 48 h, fixed with 4% paraformaldehyde for 15 min at 4°C, and incubated with mouse anti-synaptopodin (1:50) to authenticate the differentiation and

Table I. Primers used in this study.

Gene	Forward 5'-3'	Reverse 5'-3'
NLRP3	ATTACCCGCCCGAGAAAGG	TCGCAGCAAAGATCCACACAG
Caspase-1	TGGCAGGAATTCTGGAGCTT	GAGGGCAAGACGTGTACGAG
IL-1 β	TGCCACCTTTTGACAGTGATG	TGATGTGCTGCTGCGAGATT
GAPDH	AGGTCCGGTGTGAACGGATTG	TGTAGACCATGTAGTTGAGGTCC

NLRP3, NLR family pyrin domain containing 3; IL, interleukin.

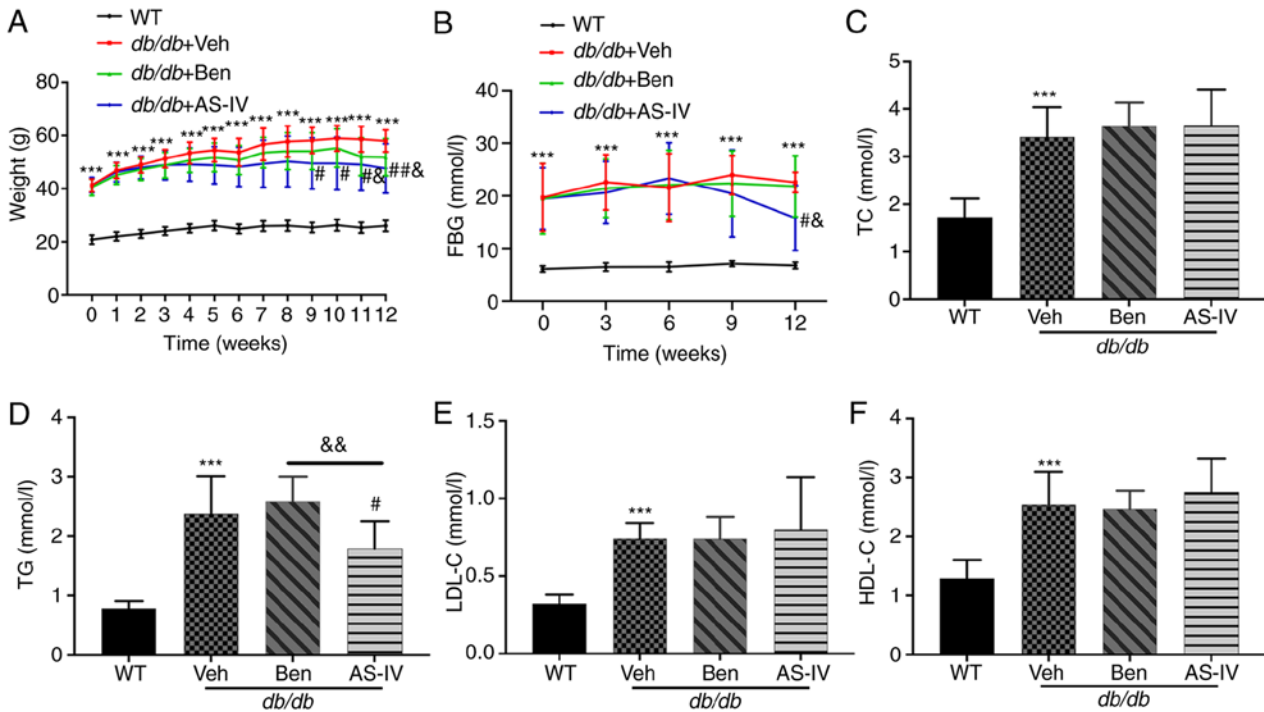


Figure 1. Effect of AS-IV on body weight, FBG and serum lipid profiles in different groups after 12 weeks of administration. (A) Weight, (B) FBG, (C) TC, (D) TG, (E) LDL-C, and (F) HDL-C. Data are presented as the mean \pm standard deviation (n=7-10). ***P<0.001 vs. WT control; *P<0.05 and **P<0.01 vs. *db/db* + vehicle; and &P<0.05 and &&P<0.01 vs. *db/db* + benazepril. AS-IV, astragaloside IV; WT, wild-type mice; FBG, fasting blood glucose; TC, total cholesterol; TG, triacylglycerol; LDL-C, low-density lipoprotein cholesterol; HDL-C, high-density lipoprotein cholesterol.

maturation. The slides were sealed using mounting medium with DAPI and then examined using the Nikon ECLIPSE Ti-S inverted fluorescence microscope (Nikon Corporation).

Western blot analysis. Total proteins were extracted from the renal cortex or mouse podocytes using precooled RIPA and PMSF (Beyotime Biotechnology) mix (99:1). The BCA protein assay kit was used to quantify the protein concentration following the manufacturer's instructions. The protein samples were then mixed with 5X loading buffer (4:1) and boiled for 5 min at 100°C. In total, 80 μ g protein was separated using 10% SDS-PAGE and transferred onto polyvinylidene fluoride membranes (0.22 μ m; EMD Millipore). The membranes were blocked using 5% skimmed milk powder in TBS with 0.1% Tween-20 for 1 h at 25°C, and incubated overnight at 4°C with the primary rabbit anti-NLRP3 (1:1,000), rabbit anti-caspase-1 (1:1,500) or rabbit anti- β -actin (1:1,000) antibodies. Following washing thrice with TBS with 0.1% Tween-20 (15 min per wash), the membranes were further incubated

with goat anti-rabbit antibody (1:2,000) for 1 h at 25°C. The super ECL solution was used (for 2 min) to develop and visualize the protein bands. The results were observed by gel imaging system (Chemi Doc XRS; Bio-Rad Laboratories, Inc.). Western blots were quantified using ImageJ software (version 1.52).

Reverse transcription-quantitative PCR (RT-qPCR). Total RNA from the renal cortex was extracted using TRIzol. RT was performed using the Revert Aid First Strand cDNA Synthesis kit according to the manufacturer's instructions. RT-qPCR was performed in the CFX96 Real-Time PCR Detection system (Bio-Rad Laboratories, Inc.) using Power SYBR™ Green PCR Master mix. The primers used are listed in Table I. The thermocycling conditions were as follows: Initial denaturation at 95°C for 10 min; followed by 40 of cycles of denaturation at 95°C for 25 sec, annealing at 55°C for 15 sec, extension at 72°C for 50 sec; and a final extension at 72°C for 5 min. GAPDH was used as an internal control (25). The relative

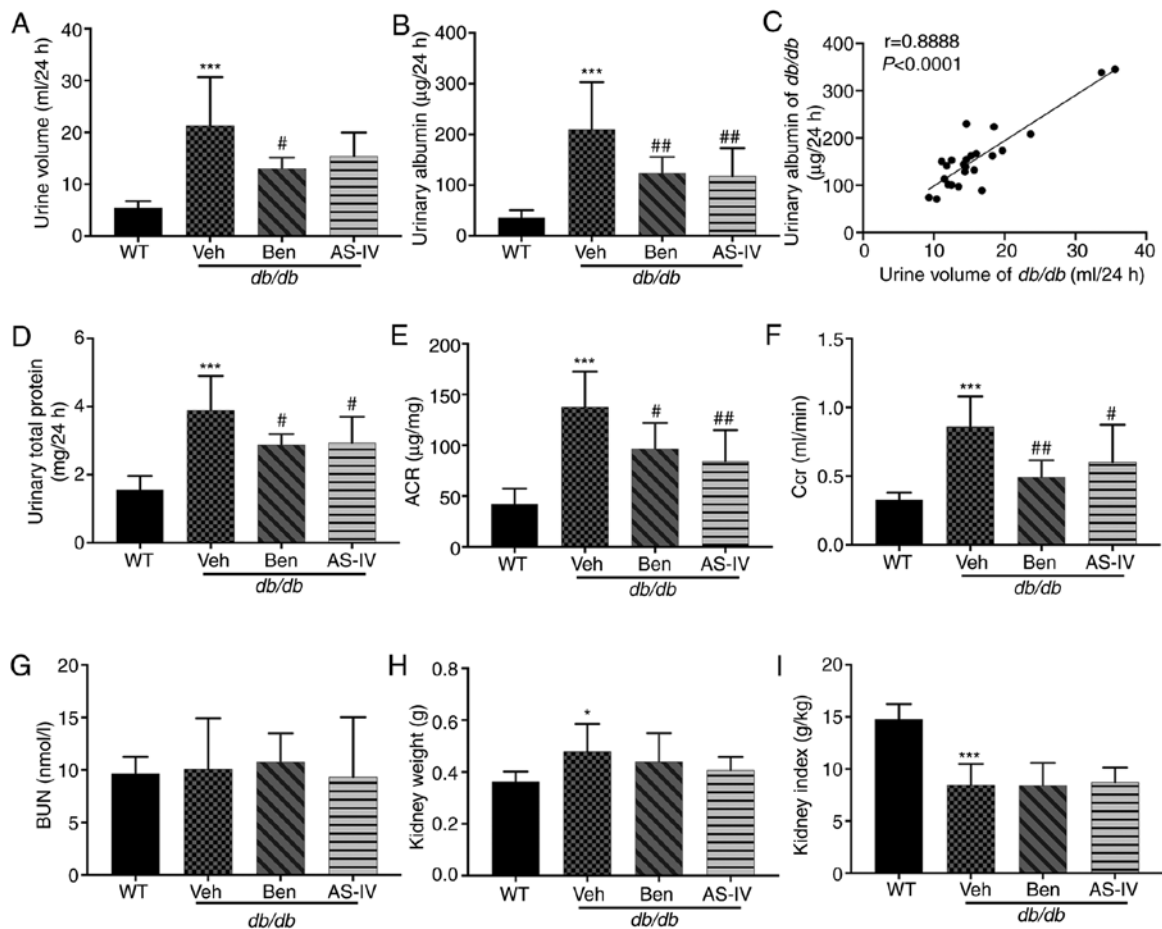


Figure 2. Benazepril and AS-IV improve renal function in *db/db* mice. (A) Urine volume; (B) urinary albumin; (C) correlation of urinary albumin with urine volume; (D) Urinary total protein; (E) ACR; (F) Ccr; (G) BUN; (H) kidney weight; (I) kidney index. Data are presented as the mean \pm standard deviation ($n=7-10$). $P<0.05$ and $***P<0.001$ vs. WT control; $^{\#}P<0.05$ and $^{\#\#}P<0.01$ vs. *db/db* + vehicle. AS-IV, astragaloside IV; WT, wild-type mice; Veh, vehicle; Ben, benazepril; Ccr, creatinine clearance rate; ACR, urinary albumin-to-creatinine ratio; BUN, blood urea nitrogen.

quantitative expression was calculated according to the $2^{-\Delta\Delta Cq}$ method (26).

Statistical analysis. Data were expressed as the mean \pm standard deviation. Statistical analysis was performed using Graphpad Prism 8 software (Graphpad Software, Inc.). One-way ANOVA, followed by Tukey's post hoc test, was used to compare differences among all groups. Correlations were assessed using the Pearson's correlation coefficient. $P<0.05$ was considered to indicate a statistically significant difference.

Results

Effects of AS-IV on body weight and metabolic markers. During the experiment, *db/db* mice exhibited a significantly increased body weight and hyperglycemia compared with the normal control mice (Fig. 1A and B; $P<0.001$). The body-weight of vehicle-treated *db/db* mice increased continuously. Starting from the 9th week, AS-IV-treated *db/db* mice exhibited a noticeable decrease in body weight (Fig. 1A; $P<0.05$). In the 12th week, the AS-IV administration group exhibited a decreasing trend in FBG compared with the vehicle- and benazepril-treated groups (Fig. 1B; $P<0.05$). However, significant

hypoglycemia and weight loss were not recorded following benazepril administration (Fig. 1A and B; $P>0.05$).

Compared with WT control mice, *db/db* mice exhibited a noticeable increase in serum TC, TG, LDL-C and HDL-C levels (Fig. 1C-F; $P<0.001$). AS-IV administration for 12 weeks significantly reduced TG levels (Fig. 1D; $P<0.05$), which were lower than those in benazepril-treated mice (Fig. 1D; $P<0.01$). In the present study, AS-IV administration did not cause a noticeable decrease in serum TC, HDL-C and LDL-C levels (Fig. 1C, E and F; $P>0.05$).

AS-IV administration protects renal function. The 24-h urine volume, urinary albumin, urinary total protein and urinary ACR were higher in *db/db* mice compared with those in WT mice; these parameters were markedly decreased in benazepril-treated mice (Fig. 2A, B, D and E; $P<0.05$ or $P<0.01$). AS-IV administration also significantly decreased urinary albumin, urinary total protein and ACR in *db/db* mice (Fig. 2B, D and E; $P<0.05$ or $P<0.01$); the 24-h urine volume demonstrated a decreasing trend, but without statistical significance (Fig. 2A; $P>0.05$). Correlation analysis between 24-h urine volume and urinary albumin indicated a significant positive correlation (Fig. 2C; $P<0.0001$). Benazepril and AS-IV administration significantly reduced Ccr levels compared with the Veh group (Fig. 2F;

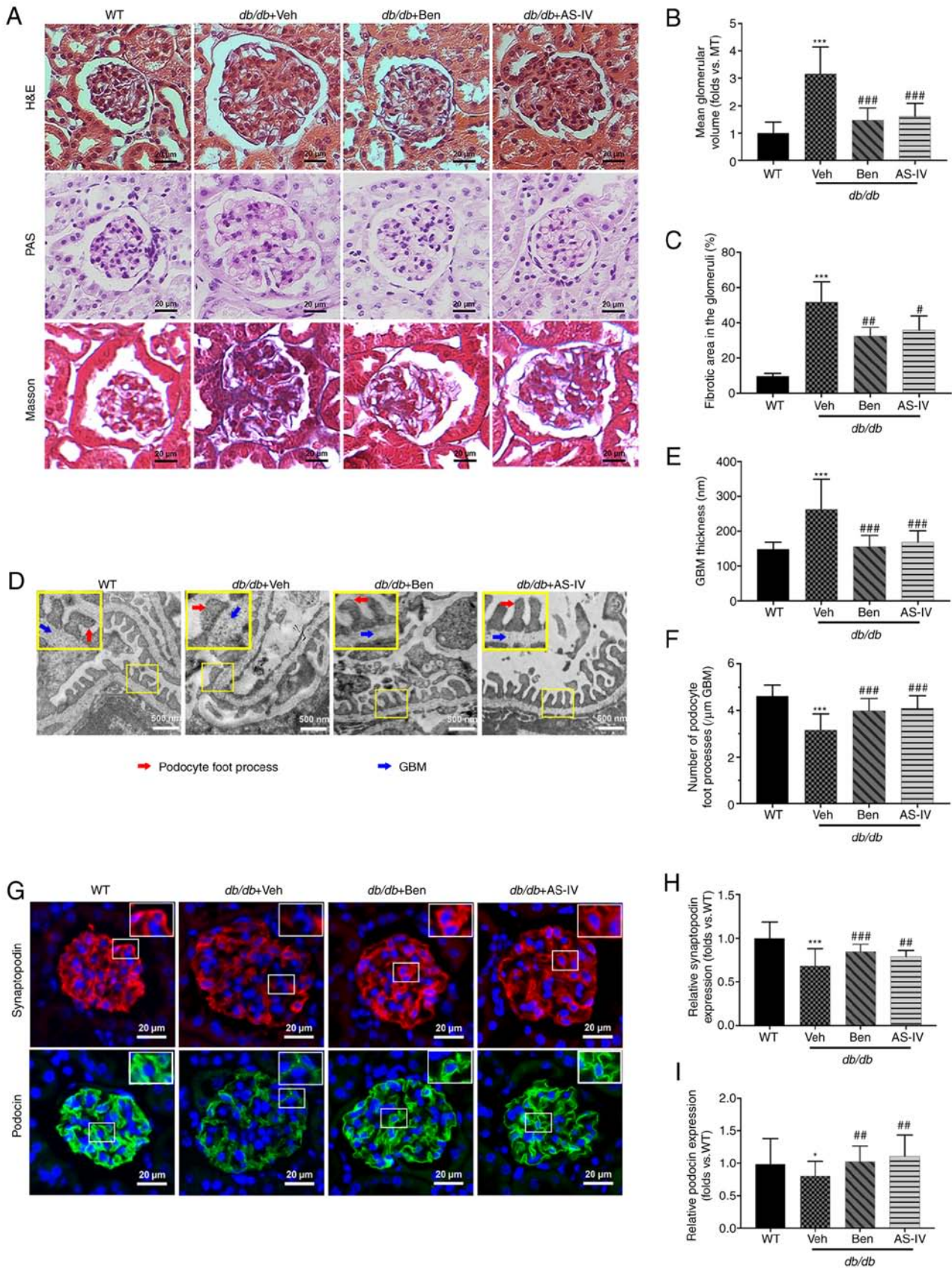


Figure 3. Benazepril and AS-IV ameliorate kidney lesions and podocyte injury in *db/db* mice. Representative images of the pathological structure of the kidneys after (A) H&E, PAS, and Masson's trichrome staining (scale bar, 20 μ m; magnification, x200). Quantitative analyses of the results for (B) mean glomerular volume and (C) fibrotic area in the glomeruli. (D) Representative images of the ultrastructure observed using TEM (scale, 500 nm; magnification, x15,000). (E) Quantification of GBM thickness and (F) number of podocyte foot processes per μ m GBM. (G) Representative immunofluorescent images of synaptopodin and podocin (scale, 20 μ m; magnification, x200). Quantification of the (H) relative expression of synaptopodin and (I) podocin in the glomeruli. Data are presented as the mean \pm standard deviation (n=3). *P<0.05 and ***P<0.001 vs. WT control; #P<0.05, ##P<0.01 and ###P<0.001 vs. *db/db* + vehicle. AS-IV, Astragaloside IV; WT, wild-type mice; Veh, vehicle; Ben, benazepril; H&E, hematoxylin and eosin; PAS, periodic acid-Schiff; GBM, glomerular basement membrane; TEM, transmission electron microscopy.

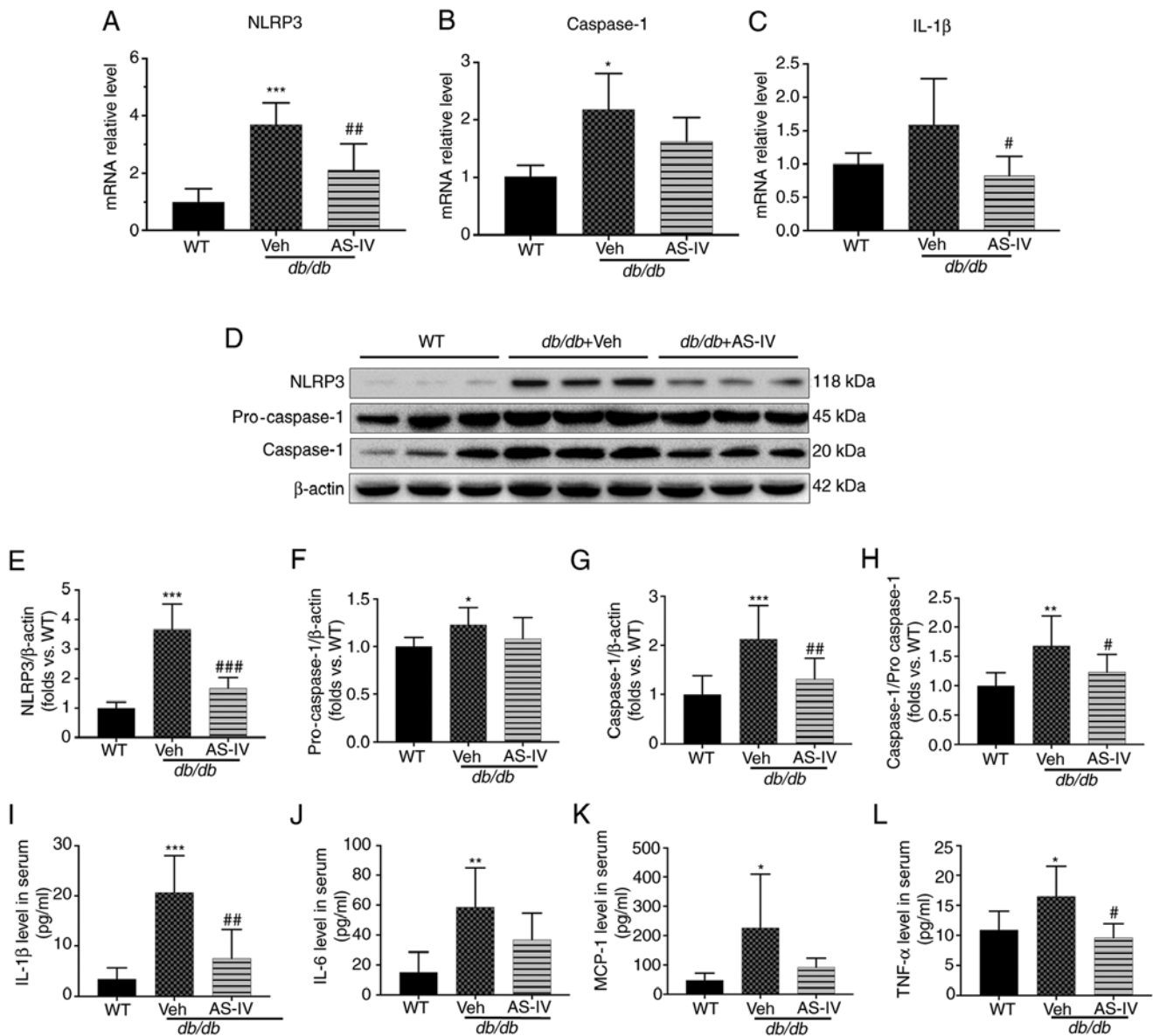


Figure 4. AS-IV inhibits NLRP3 inflammasome activation in the renal cortex of *db/db* mice. The mRNA levels of (A) NLRP3, (B) caspase-1, and (C) IL-1 β . (D) Western blot analysis of NLRP3, pro-caspase-1 and caspase-1. The protein levels of (E) NLRP3, (F) pro-caspase-1, and (G) caspase-1 were normalized to β -actin protein level. (H) Ratio of the protein level of caspase-1 to that of pro-caspase-1. The levels of (I) IL-1 β , (J) IL-6, (K) MCP-1, and (L) TNF- α in serum. Data are presented as the mean \pm standard deviation. (A-C and I-L) $n=6-7$; (E-H) $n=3$. * $P<0.05$, ** $P<0.01$ and *** $P<0.001$ vs. WT mice; # $P<0.05$, ## $P<0.01$ and ### $P<0.001$ vs. *db/db* + vehicle. WT, wild-type mice; Veh: Vehicle; AS-IV, Astragaloside IV; NLRP3, NLR family pyrin domain containing 3; IL, interleukin; TNF, tumor necrosis factor; MCP-1, monocyte chemoattractant protein-1.

$P<0.05$ or $P<0.01$). The kidney weight of *db/db* mice was higher than that of WT mice (Fig. 2H; $P<0.05$), indicating renal hypertrophy in the former. However, the reduction in kidney weight and index following AS-IV administration was not significant (Fig. 2H and I; $P>0.05$). No changes in BUN levels were observed among different groups (Fig. 2G; $P>0.05$).

AS-IV ameliorates renal histopathology and podocyte injury. Histological examination revealed that *db/db* mice displayed glomerular hypertrophy, obvious mesangial proliferation, increased extracellular matrix (ECM) deposition and severe renal fibrosis at 20 weeks compared with the WT control mice (Fig. 3A). The glomerular volume and fibrotic area in the glomeruli of *db/db* mice were higher than those in WT mice (Fig. 3B and C; $P<0.001$). AS-IV- and benazepril-treated

groups revealed a significant reduction in the mean glomerular volume and fibrotic area in the glomeruli compared with *db/db* mice treated with vehicle alone (Fig. 3B and C; $P<0.05$, $P<0.01$ or $P<0.001$).

TEM images revealed that vehicle-treated *db/db* mice presented extensive podocyte foot process fusion, podocyte foot process widening, podocyte loss and GBM thickening compared with the control mice (Fig. 3D). GBM thickness was attenuated by AS-IV or benazepril administration (Fig. 3E; $P<0.001$). In addition, the number of podocyte foot processes per μm of GBM was higher in both AS-IV- and benazepril-treated mice than in *db/db* mice treated with vehicle alone (Fig. 3F; $P<0.001$).

To further evaluate the effect of AS-IV on podocytes in *db/db* mice, immunofluorescence staining of synaptopodin

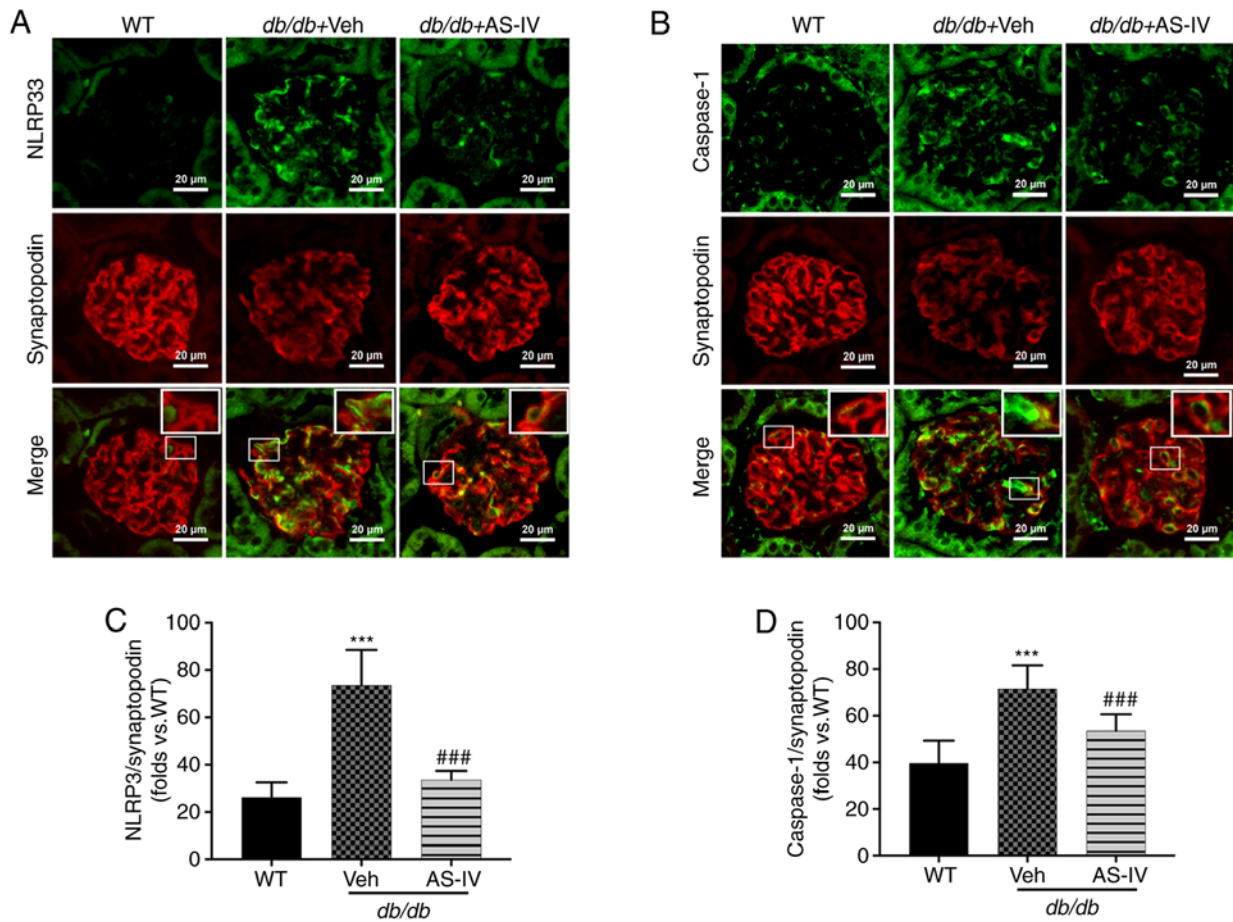


Figure 5. AS-IV mitigates NLRP3 inflammasome activation in podocytes of the glomeruli of *db/db* mice. Colocalization of (A) NLRP3 with synaptopodin and (B) caspase-1 with synaptopodin (a podocyte marker) in the glomeruli of WT control mice, and vehicle- and AS-IV-treated mice (scale bar, 20 μ m; magnification, x200). Mean fluorescence intensity of (C) NLRP3 with synaptopodin and (D) caspase-1 with synaptopodin in the glomeruli. Data are presented as the mean \pm standard deviation (n=3). ***P<0.001 vs. WT control; and ###P<0.001 vs. *db/db* + vehicle. WT, wild-type mice; Veh, vehicle; AS-IV, Astragaloside IV; NLRP3, NLR family pyrin domain containing 3.

and podocin (the podocyte markers in the glomeruli) was performed. As revealed in Fig. 3G, immunofluorescence revealed intense and linear staining of both podocin and synaptopodin in WT controls. This expression pattern was weak and discontinuous in vehicle-treated *db/db* mice. Moreover, the relative expression of both podocin and synaptopodin was significantly decreased in vehicle-treated *db/db* mice compared with that in WT mice (Fig. 3H and I; P<0.05 or P<0.001); this effect was partly reversed by AS-IV and benazepril administration (Fig. 3H and I; P<0.01 or P<0.001).

AS-IV inhibits NLRP3 inflammasome-mediated inflammation in the renal cortex and serum. To explore the protective mechanism of AS-IV, the gene expression of NLRP3, caspase-1 and IL-1 β in the renal cortex of vehicle- and AS-IV-treated *db/db* and WT mice was firstly determined. The mRNA levels of NLRP3 and caspase-1 were significantly higher in the vehicle-treated mice than in the WT mice, as revealed by RT-qPCR (Fig. 4A and B; P<0.001 and P<0.05, respectively). However, the IL-1 β level exhibited an increasing trend, with no significant difference (Fig. 4C; P=0.0872). Following treatment with AS-IV for 12 weeks, the gene expression of NLRP3 and IL-1 β was significantly reduced (Fig. 4A and C;

P<0.01 and P<0.05, respectively). Next, the protein expression of NLRP3 and caspase-1 in the renal cortex and IL-1 β in the serum were detected (Fig. 4D-I). An increased activation of NLRP3, pro-caspase-1, caspase-1 and IL-1 β was observed in the vehicle-treated group (Fig. 4E-I; P<0.05, P<0.01 or P<0.001). AS-IV administration inhibited the levels of NLRP3, caspase-1 and IL-1 β and reduced the caspase-1 to pro-caspase-1 ratio (Fig. 4E and G-I; P<0.05, P<0.01 or P<0.001); a decreasing trend was observed in pro-caspase-1, but without statistical significance (Fig. 4F; P>0.05).

Furthermore, the expression of certain downstream inflammatory cytokines of IL-1 β , including IL-6, TNF- α and MCP-1 (10,11), was detected in the serum. The expression of these cytokines increased in vehicle-treated *db/db* mice compared with that in WT mice (P<0.05 or P<0.01; Fig. 4J-L). AS-IV administration significantly reduced TNF- α levels (P<0.05; Fig. 4L), but the reduction in IL-6 and MCP-1 levels was not significant (P=0.1775 and P=0.1119, respectively; Fig. 4J and K).

AS-IV inhibits NLRP3 inflammasome activation in podocytes from *db/db* mice. NLRP3 and caspase-1 were localized within the podocytes of mouse renal tissue, as revealed by double immunofluorescence staining. Synaptopodin was used

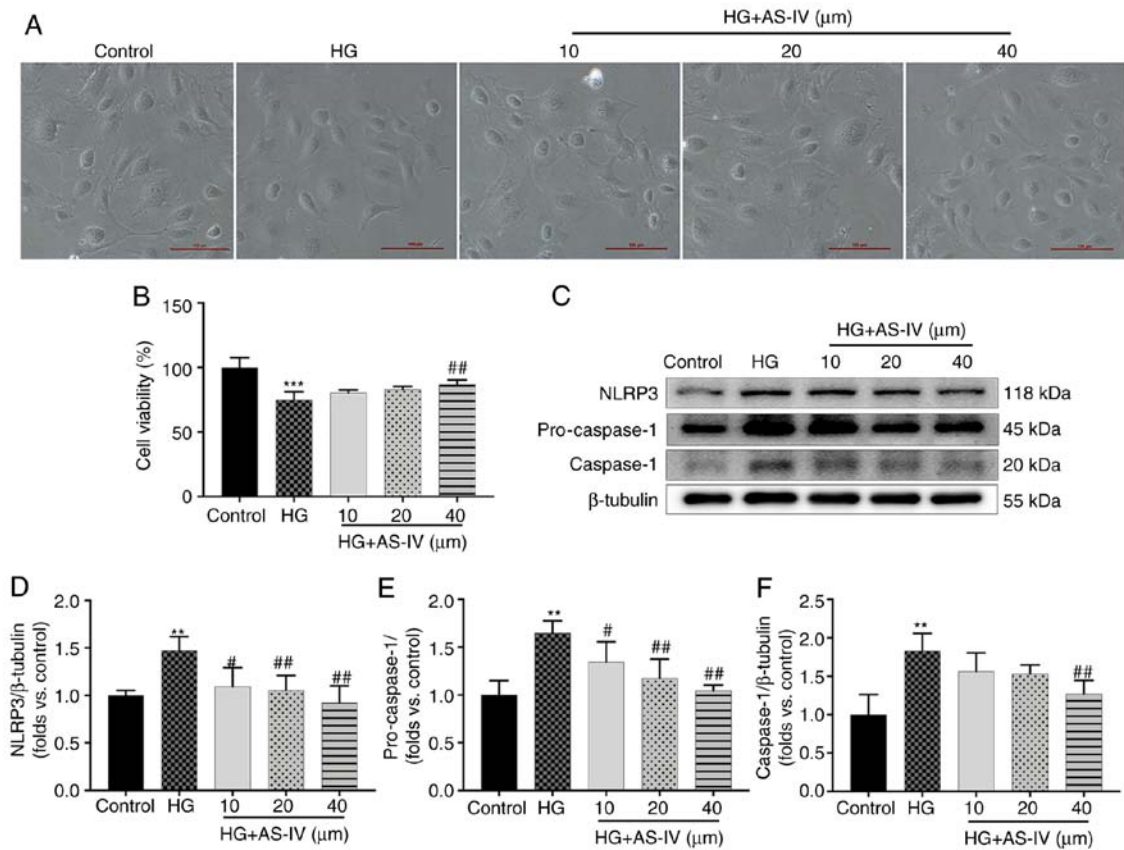


Figure 6. AS-IV inhibits HG-induced decrease in cell viability and NLRP3 inflammasome activation in podocytes. (A) Morphological images of each group of podocytes (scale bar, 100 μm; magnification, x100). (B) Podocytes were cultured with different concentration of AS-IV (10, 20, or 40 μM) for 24 h and the cell viability was assessed using MTT assays. (C) Western blot analysis of NLRP3, pro-caspase-1, and caspase-1. The protein levels of (D) NLRP3, (E) pro-caspase-1, and (F) caspase-1 were normalized to β-tubulin protein level. Data are presented as the mean ± standard deviation (n=3). **P<0.01 and ***P<0.001 vs. the control; #P<0.05 and ##P<0.01 vs. HG. Control, normal glucose; HG, high glucose; AS-IV, Astragaloside IV; NLRP3, NLR family pyrin domain containing 3.

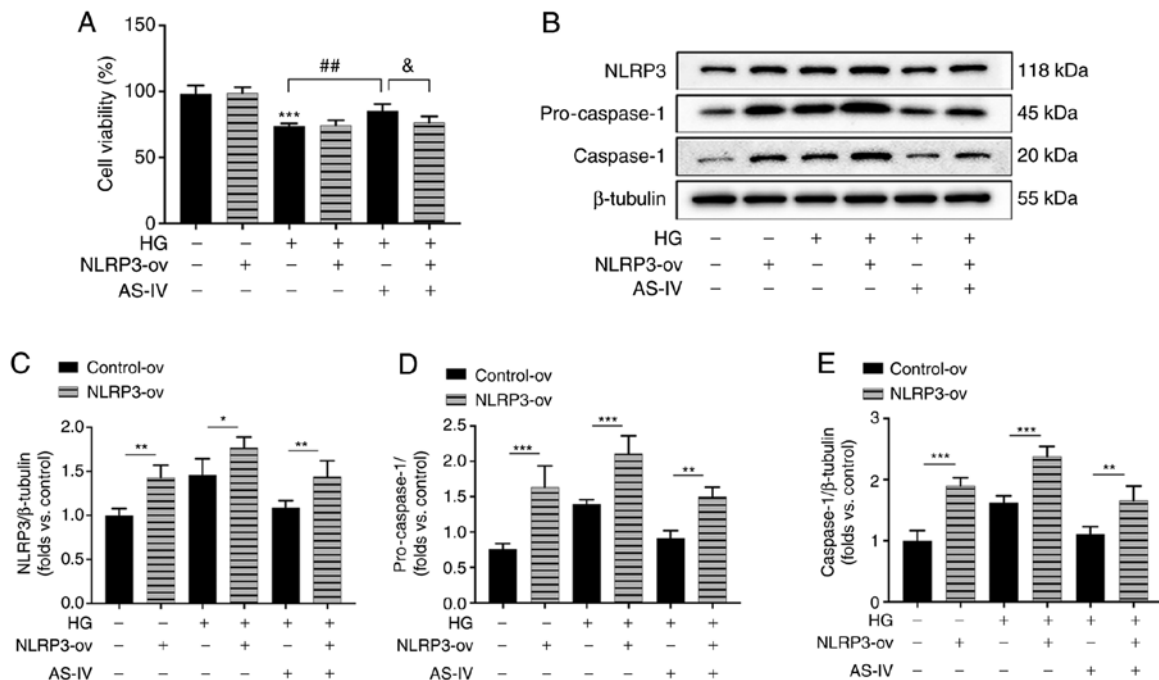


Figure 7. AS-IV inhibits HG-induced cell viability decrease and NLRP3 inflammasome activation in podocytes. (A) Podocytes were transfected with the recombinant lentiviral vectors for NLRP3 and empty vector, and the cell viability was assessed using an MTT assay. (B) Western blot analysis of NLRP3, pro-caspase-1, and caspase-1. The protein levels of (C) NLRP3, (D) pro-caspase-1, and (E) caspase-1 were normalized to the β-tubulin protein level. Data are presented as the mean ± standard deviation. (A, C-E) n=3. *P<0.05, **P<0.01 and ***P<0.001; ##P<0.01 and &P<0.05. AS-IV, Astragaloside IV; HG, high glucose; NLRP3, NLR family pyrin domain containing 3; NLRP3-ov, NLRP3 overexpression.

as the podocyte marker. The colocalization of NLRP3 and caspase-1 with synaptopodin was observed using confocal microscopy. Colocalization was increased in the glomeruli of vehicle-treated *db/db* mice compared with that in the glomeruli of WT mice. The expression levels of NLRP3 and caspase-1 were significantly increased, while that of synaptopodin was decreased in the glomeruli of vehicle-treated *db/db* mice (Fig. 5A and B). However, AS-IV administration significantly reduced the mean fluorescence intensity of both NLRP3 with synaptopodin and caspase-1 with synaptopodin in the glomeruli of *db/db* mice ($P < 0.001$; Fig. 5C and D).

AS-IV inhibits the decrease in cell viability and NLRP3 inflammasome activation in HG-induced podocytes. Podocytes cultured for 2 days at 37°C in medium without recombinant murine γ -interferon express no or low levels of synaptopodin (Fig. S1A), but the podocytes cultured for 10 days at 37°C express high levels of synaptopodin (Fig. S1B). On days 10–14, large, differentiated arborized podocytes with well-developed prominent processes could be observed and there was no significant difference in the morphology of podocytes among different groups (Fig. 6A). However, the cell viability of podocytes was significantly decreased after a 24-h stimulation with HG (Fig. 6B, $P < 0.001$), which was reversed by treatment with 40 μ M AS-IV for 24 h (Fig. 6B; $P < 0.01$), while treatment with 10 and 20 μ M AS-IV did not influence cell viability (Fig. 6B; $P > 0.05$). The protein expression of NLRP3, pro-caspase-1, and cleaved caspase-1 was also detected (Fig. 6C). Podocytes in the HG group exhibited higher protein levels of NLRP3, pro-caspase-1 and caspase-1 than those in the control group (Fig. 6D–F; $P < 0.01$), which were significantly decreased by 40 μ M AS-IV treatment ($P < 0.01$). In addition, 10 and 20 μ M AS-IV treatment also significantly inhibited the levels of NLRP3 and pro-caspase-1 ($P < 0.05$ or $P < 0.01$), while the reduction of caspase-1 was not significant (Fig. 6D–F; $P > 0.05$).

AS-IV attenuates HG-induced podocyte injury by inhibiting NLRP3 inflammasome activation. To further confirm the role of NLRP3 inflammasome in the protective effect of AS-IV on HG-induced podocyte injury, NLRP3 was overexpressed in podocytes by the recombinant lentivirus vectors for NLRP3. The increase of cell viability following AS-IV administration was revealed to be inhibited by NLRP3 overexpression (Fig. 7A). The protein expression levels of NLRP3, pro-caspase-1 and active caspase-1 in NLRP3-ov groups were significantly increased compared with those in the control-ov groups (Fig. 7B–E). HG induced an obvious activation of NLRP3, pro-caspase-1 and caspase-1 which were inhibited by AS-IV treatment, while these inhibitory effects were all abolished by NLRP3 overexpression (Fig. 7B–E). These results indicated that AS-IV attenuated HG-induced podocyte injury by inhibiting NLRP3 inflammasome activation.

Discussion

Proteinuria is the primary diagnostic and post-treatment evaluation marker of progressive kidney damage (2). ACR is an important marker for the evaluation of urinary albumin excretion and early renal function decline in DN (27). A

previous study established that albumin excretion rates were 8–62-fold higher in *db/db* mice than that in control mice at the age of 8 weeks (16). In the present study, the 24-h urine volume, urinary total protein and ACR levels were higher in *db/db* mice than in WT mice at 20 weeks. These results confirmed that *db/db* mice presented with nephropathy.

Obesity, hyperglycemia and dyslipidemia are currently considered major risk factors for DN (28). AS-IV was revealed to effectively reduce weight gain, hyperglycemia and serum TG levels in *db/db* mice. It was also revealed that AS-IV could reduce 24-h urinary albumin levels and ACR. In addition, the positive correlation between urinary albumin and urinary volume indicated that the mice in the present study exhibited glomerular hyperfiltration in DN. AS-IV reduced the elevated Ccr levels in *db/db* mice, mitigating renal hypertrophy and glomerular hyperfiltration. However, the BUN level was not significantly increased. These results demonstrated that 20-week-old *db/db* mice were still in the early stage of DN and that AS-IV is an effective therapeutic option for DN.

Structural lesions, including glomerular hypertrophy, thickened GBM, increased ECM deposition and glomerulosclerosis, are involved in progressive proteinuria in DN (29). In addition, podocyte injury has been confirmed to be a key event that may lead to glomerulosclerosis and proteinuria, as it represents renal function decline in DN (30). Podocytes are terminally differentiated epithelial cells that are infrequently able to divide once damaged (31). In that respect, the pathological changes in glomeruli were firstly observed using various staining techniques. The results indicated that AS-IV administration attenuated glomerular injury, including glomerular mesangial cell proliferation, ECM deposition and renal fibrosis, in *db/db* mice. The ultrastructure of glomeruli was further observed by TEM. Foot process fusion, foot process widening, podocyte loss and GBM thickening were aggravated in *db/db* mice. All these changes were suppressed following AS-IV administration. In addition, the expression levels of podocyte markers, including podocin and synaptopodin, were detected and revealed to be significantly reduced in vehicle-treated *db/db* mice. These changes indicated that *db/db* mice exhibited significant podocyte injury at 20 weeks. In the present study, the activation of podocin and synaptopodin was demonstrated in AS-IV-treated *db/db* mice, which confirmed that AS-IV prevents the progression of DN by protecting podocytes.

Several studies have indicated that inflammation plays an indispensable role in the progression of DN (9,32). The NLRP3 inflammasome, a key component of innate immunity maintenance, can be activated by several factors, including chronic hyperglycemia, obesity and reactive oxygen species, which in turn activate pro-inflammatory mediators such as IL-1 β , resulting in diabetic renal damage (5). A study has reported that NLRP3 inflammation activation occurs at an early stage of nephropathy in *db/db* mice and is accompanied by podocyte injury, which is associated with the increase in ALB of *db/db* mice (6). In the present study, the expression of NLRP3 and caspase-1 was higher in the renal cortex, podocytes of the glomeruli of *db/db* mice and mouse podocytes incubated with HG *in vitro*. Caspase-1-dependent inflammasome activation plays a crucial role in DN initiation (33). NLRP3 can promote IL-1 β induction by cleaving caspase-1 (8). The IL-1 β level in

the serum was also increased in vehicle-treated mice. AS-IV administration reduced the expression levels of NLRP3, caspase-1 and IL-1 β , and decreased the colocalization of both NLRP3 with synaptopodin and caspase-1 with synaptopodin in the glomeruli of *db/db* mice. Further experiments revealed that AS-IV administration also inhibited NLRP3 activation in HG-induced mouse podocytes *in vitro*, while these protective effects were blunted by NLRP3 overexpression. These results indicated that AS-IV *db/db* exerted its therapeutic effect on DN by inhibiting NLRP3 inflammasome activation in podocytes.

In addition, it was also observed that serum levels of IL-6, MCP-1 and TNF- α , which are downstream inflammatory cytokines of IL-1 β , were increased in *db/db* mice treated with vehicle alone. Multiple studies have confirmed that the levels of IL-6, TNF- α and MCP-1 are correlated with albuminuria excretion in patients with DM and DN (34,35). These inflammatory cytokines can further recruit macrophages to accumulate in the kidney tissues, which release more pro-inflammatory factors and enhance the inflammatory response (10,36). AS-IV administration reduced the serum levels of IL-6, MCP-1 and TNF- α , particularly those of TNF- α . These results suggested that AS-IV could reduce inflammatory reaction in the kidney and serum of *db/db* mice.

In conclusion, it was demonstrated herein that AS-IV can reduce weight gain, mitigate glucolipid metabolism disorders and protect the kidney against proteinuria and podocyte injury in *db/db* mice, likely through anti-NLRP3 inflammasome-mediated inflammation. These findings indicated that AS-IV, a natural food supplement, could become an effective therapeutic option for T2DM-associated nephropathy. AS-IV may have a wide application prospect in the field of medicine due to the high prevalence of dyslipidemia and obesity among patients with T2DM (37). However, experiments in fatty acid-induced cells were not performed, which was one limitation in this study. In future studies, the role of AS-IV on podocytes in high palmitic acid *in vitro* will further be explored.

Acknowledgements

Not applicable.

Funding

The present study was supported by the Priority Academic Program Development of Jiangsu Higher Education Institutions (Integration of Chinese and Western Medicine) and the International Science and Technology Cooperation Program of China (grant no. 2010DFA31620).

Availability of data and materials

The datasets generated during and/or analyzed during the current study are available from the corresponding author on reasonable request.

Authors' contributions

XL, XZ, and HF designed the study. XZ, HF, YT, BK and SF conducted the experiments. HF analyzed the data and

wrote the manuscript. HF, XZ, YT, BK, and SF reviewed and edited the manuscript. All authors read and approved the final manuscript.

Ethics approval and consent to participate

All animal experiments were approved (approval no. IACUC-GAMH-2019-010) by the Animal Ethics Committee of Guang'anmen Hospital, Chinese Academy of Traditional Chinese Medicine (Beijing, China) and the procedures were consistent with the guidelines of the Committee.

Patient consent for publication

Not applicable.

Competing interests

The authors declare that they have no competing interests.

References

- Alicic RZ, Rooney MT and Tuttle KR: Diabetic kidney disease: Challenges, progress, and possibilities. *Clin J Am Soc Nephrol* 12: 2032-2045, 2017.
- Liew A, Bavanandan S, Prasad N, Wong MG, Chang JM, Eiam-Ong S, Hao CM, Lim CY, Lim SK, Oh KH, *et al*: Asian pacific society of nephrology clinical practice guideline on diabetic kidney disease. *Nephrology (Carlton)* 25 (Suppl 2): S12-S45, 2020.
- Lin JS and Susztak K: Podocytes: The weakest link in diabetic kidney disease? *Curr Diab Rep* 16: 45, 2016.
- Nichols GA, Déruaz-Luyet A, Brodovicz KG, Kimes TM, Rosales AG and Hauske SJ: Kidney disease progression and all-cause mortality across estimated glomerular filtration rate and albuminuria categories among patients with vs. without type 2 diabetes. *BMC Nephrol* 21: 167, 2020.
- Hou Y, Lin S, Qiu J, Sun W, Dong M, Xiang Y, Wang L and Du P: NLRP3 inflammasome negatively regulates podocyte autophagy in diabetic nephropathy. *Biochem Biophys Res Commun* 521: 791-798, 2020.
- Shahzad K, Bock F, Dong W, Wang H, Kopf S, Kohli S, Al-Dabet MM, Ranjan S, Wolter J, Biemann R, *et al*: Nlrp3-inflammasome activation in non-myeloid-derived cells aggravates diabetic nephropathy. *Kidney Int* 87: 74-84, 2015.
- Karki R and Kanneganti TD: Diverging inflammasome signals in tumorigenesis and potential targeting. *Nat Rev Cancer* 19: 197-214, 2019.
- Liu D, Zeng X, Li X, Cui C, Hou R, Guo Z, Mehta JL and Wang X: Advances in the molecular mechanisms of NLRP3 inflammasome activators and inactivators. *Biochem Pharmacol* 175: 113863, 2020.
- Wu M, Han W, Song S, Du Y, Liu C, Chen N, Wu H, Shi Y and Duan H: NLRP3 deficiency ameliorates renal inflammation and fibrosis in diabetic mice. *Mol Cell Endocrinol* 478: 115-125, 2018.
- Navarro-Gonzalez JF, Mora-Fernandez C, Muros de Fuentes M and Garcia-Perez J: Inflammatory molecules and pathways in the pathogenesis of diabetic nephropathy. *Nat Rev Nephrol* 7: 327-340, 2011.
- Chen J, Xuan J, Gu YT, Shi KS, Xie JJ, Chen JX, Zheng ZM, Chen Y, Chen XB, Wu YS, *et al*: Celastrol reduces IL-1 β induced matrix catabolism, oxidative stress and inflammation in human nucleus pulposus cells and attenuates rat intervertebral disc degeneration *in vivo*. *Biomed Pharmacother* 91: 208-219, 2017.
- Ju Y, Su Y, Chen Q, Ma K, Ji T, Wang Z, Li W and Li W: Protective effects of Astragaloside IV on endoplasmic reticulum stress-induced renal tubular epithelial cells apoptosis in type 2 diabetic nephropathy rats. *Biomed Pharmacother* 109: 84-92, 2019.
- Zhang Z, Wang J, Zhu Y, Zhang H and Wang H: Astragaloside IV alleviates myocardial damage induced by type 2 diabetes via improving energy metabolism. *Mol Med Rep* 20: 4612-4622, 2019.

14. Li L, Hou X, Xu R, Liu C and Tu M: Research review on the pharmacological effects of astragaloside IV. *Fundam Clin Pharmacol* 31: 17-36, 2017.
15. Leng B, Zhang Y, Liu X, Zhang Z, Liu Y, Wang H and Lu M: Astragaloside IV suppresses high glucose-induced NLRP3 inflammasome activation by inhibiting TLR4/NF- κ B and CaSR. *Mediators Inflamm* 2019: 1082497, 2019.
16. Sharma K, McCue P and Dunn SR: Diabetic kidney disease in the db/db mouse. *Am J Physiol Renal Physiol* 284: F1138-F1144, 2003.
17. Sun H, Wang W, Han P, Shao M, Song G, Du H, Yi T and Li S: Astragaloside IV ameliorates renal injury in db/db mice. *Sci Rep* 6: 32545, 2016.
18. Chen H, Zhang X, Liu L, Cai M, Guo Z and Qiu L: Application of red clover isoflavone extract as an adjuvant in mice. *Exp Ther Med* 19: 1175-1182, 2020.
19. Jiang L, Cui H and Ding J: Smad3 signalling affects high glucose-induced podocyte injury via regulation of the cytoskeletal protein transgelin. *Nephrology (Carlton)* 25: 659-666, 2020.
20. Li F, Chen Y, Li Y, Huang M and Zhao W: Geniposide alleviates diabetic nephropathy of mice through AMPK/SIRT1/NF- κ B pathway. *Eur J Pharmacol* 886: 173449, 2020.
21. Ma Y, Li W, Yazdizadeh Shotorbani P, Dubansky BH, Huang L, Chaudhari S, Wu P, Wang LA, Ryou MG, Zhou Z and Ma R: Comparison of diabetic nephropathy between male and female eNOS(-/-) db/db mice. *Am J Physiol Renal Physiol* 316: F889-F897, 2019.
22. Lane PH, Steffes MW and Mauer SM: Estimation of glomerular volume: A comparison of four methods. *Kidney Int* 41: 1085-1089, 1992.
23. Canaud G, Bienaimé F, Viau A, Treins C, Baron W, Nguyen C, Burtin M, Berissi S, Giannakakis K, Muda AO, *et al.*: AKT2 is essential to maintain podocyte viability and function during chronic kidney disease. *Nat Med* 19: 1288-1296, 2013.
24. Zhan Y, Zhou Y, Zheng W, Liu W, Wang C, Lan X, Deng X, Xu Y, Zhang B and Ning Y: Alterations of multiple peripheral inflammatory cytokine levels after repeated ketamine infusions in major depressive disorder. *Transl Psychiatry* 10: 246, 2020.
25. Kuo CW, Shen CJ, Tung YT, Chen HL, Chen YH, Chang WH, Cheng KC, Yang SH and Chen CM: Extracellular superoxide dismutase ameliorates streptozotocin-induced rat diabetic nephropathy via inhibiting the ROS/ERK1/2 signaling. *Life Sci* 135: 77-86, 2015.
26. Livak KJ and Schmittgen TD: Analysis of relative gene expression data using real-time quantitative PCR and the 2(-Delta Delta C(T)) method. *Methods* 25: 402-408, 2001.
27. Nowak N, Skupien J, Smiles AM, Yamanouchi M, Niewczas MA, Galecki AT, Duffin KL, Breyer MD, Pullen N, Bonventre JV and Krolewski AS: Markers of early progressive renal decline in type 2 diabetes suggest different implications for etiological studies and prognostic tests development. *Kidney Int* 93: 1198-1206, 2018.
28. Tziomalos K and Athyros VG: Diabetic nephropathy: New risk factors and improvements in diagnosis. *Rev Diabet Stud* 12: 110-118, 2015.
29. Kanwar YS, Sun L, Xie P, Liu FY and Chen S: A glimpse of various pathogenetic mechanisms of diabetic nephropathy. *Annu Rev Pathol* 6: 395-423, 2011.
30. Weil EJ, Lemley KV, Mason CC, Yee B, Jones LI, Blouch K, Lovato T, Richardson M, Myers BD and Nelson RG: Podocyte detachment and reduced glomerular capillary endothelial fenestration promote kidney disease in type 2 diabetic nephropathy. *Kidney Int* 82: 1010-1017, 2012.
31. Barisoni L and Mundel P: Podocyte biology and the emerging understanding of podocyte diseases. *Am J Nephrol* 23: 353-360, 2003.
32. Wada J and Makino H: Innate immunity in diabetes and diabetic nephropathy. *Nat Rev Nephrol* 12: 13-26, 2016.
33. Shahzad K, Bock F, Al-Dabet MM, Gadi I, Kohli S, Nazir S, Ghosh S, Ranjan S, Wang H, Madhusudhan T, *et al.*: Caspase-1, but not caspase-3, promotes diabetic nephropathy. *J Am Soc Nephrol* 27: 2270-2275, 2016.
34. Perlman AS, Chevalier JM, Wilkinson P, Liu H, Parker T, Levine DM, Sloan BJ, Gong A, Sherman R and Farrell FX: Serum inflammatory and immune mediators are elevated in early stage diabetic nephropathy. *Ann Clin Lab Sci* 45: 256-263, 2015.
35. Murakoshi M, Gohda T and Suzuki Y: Circulating tumor necrosis factor receptors: A potential biomarker for the progression of diabetic kidney disease. *Int J Mol Sci* 21: 1957, 2020.
36. Chow FY, Nikolic-Paterson DJ, Ma FY, Ozols E, Rollins BJ and Tesch GH: Monocyte chemoattractant protein-1-induced tissue inflammation is critical for the development of renal injury but not type 2 diabetes in obese db/db mice. *Diabetologia* 50: 471-480, 2007.
37. Narindrarangkura P, Bosl W, Rangsinsin R and Hatthachote P: Prevalence of dyslipidemia associated with complications in diabetic patients: A nationwide study in Thailand. *Lipids Health Dis* 18: 90, 2019.



This work is licensed under a Creative Commons Attribution-NonCommercial-NoDerivatives 4.0 International (CC BY-NC-ND 4.0) License.